Biogeosciences Discuss., 9, 14639–14687, 2012
www.biogeosciences-discuss.net/9/14639/2012/
doi:10.5194/bgd-9-14639-2012


Biogeosciences Discussions



# Spatial scale dependency of the modelled climatic response to deforestation

**P. Longobardi**[1,2], **A. Montenegro**[1,3], **H. Beltrami**[1,2], **and M. Eby**[4]

[1]Climate and Atmospheric Sciences Institute (CASI), Canada
[2]Department of Earth Sciences, St. Francis Xavier University, Antigonish, NS, Canada
[3]Department of Geography, Ohio State University, Columbus, Ohio, USA
[4]School of Earth and Ocean Sciences, University of Victoria, Victoria, British Columbia, Canada

Received: 24 September 2012 – Accepted: 10 October 2012 – Published: 22 October 2012

Correspondence to: A. Montenegro (montenegro.8@osu.edu) and
H. Beltrami (hbeltram@stfx.ca)

Published by Copernicus Publications on behalf of the European Geosciences Union.







## Abstract

Deforestation is associated with increased atmospheric $CO_2$ and alterations to the surface energy and mass balances that can lead to local and global climate changes. Previous modelling studies show that the global surface air temperature (SAT) response to deforestation depends on latitude, with most simulations showing that high latitude deforestation results in cooling, low latitude deforestation causes warming and that the mid latitude response is mixed. These earlier conclusions are based on simulated large scale land cover change, with complete removal of trees from whole latitude bands. Using a global climate model we determine effects of removing fractions of 5 % to 100 % of forested areas in the high, mid and low latitudes. All high latitude deforestation scenarios reduce mean global SAT, the opposite occurring for low latitude deforestation, although a decrease in SAT is registered over low latitude deforested areas. Mid latitude SAT response is mixed. For all simulations deforested areas tend to become drier and have lower surface air temperature, although soil temperatures increase over deforested mid and low latitude grid cells. For high latitude deforestation fractions of 45 % and above, larger net primary productivity, in conjunction with colder and drier conditions after deforestation, cause an increase in soil carbon large enough to generate a previously not reported net drawdown of $CO_2$ from the atmosphere. Our results support previous indications of the importance of changes in cloud cover in the modelled temperature response to deforestation at low latitudes. They also show the complex interaction between soil carbon dynamics and climate and the role this plays on the climatic response to land cover change.

## 1 Introduction

Agricultural lands occupy approximately 38 % of the Earth's land surface (Ramankutty et al., 2008). These croplands and pastures presently cover about 10 %, 45 % and 27 % of the areas originally occupied by boreal, temperate, and tropical forests respectively





BGD
9, 14639–14687, 2012



(Ramankutty and Foley, 1999; Ramankutty et al., 2008; Monfreda et al., 2008; Foley et al., 2011). Population growth and the associated expansion of agricultural lands is the primary cause of present day deforestation (Gibbs et al., 2010; Foley et al., 2011). Although rates of deforestation have decreased over the last decade, the loss of forested areas is expected to continue during the present century (Magrin et al., 2007; Food and A. O. of the United Nations, 2010). Forested area in the Amazon Basin, where the largest rainforest on Earth is found, could be reduced in approximately 50 % by 2050. (Butler, 2006; Magrin et al., 2007; Food and A. O. of the United Nations, 2010).

While most deforestation occurs in the tropics, non-tropical forests are likely to suffer new deforestation pressures as the climate warms and areas which were previously too cold become suitable for agriculture (McCarthy et al., 2001; Walker and Sydneysmith, 2007).

Assuming recent rates of human population growth are maintained until the end of the century, the Earth's population will approach 10 billion around 2100. With current population to agriculture density of $\sim$ 147 people per km$^2$, to meet the same quantity of food availability as present day, with no increases in productivity through technological advances, by 2100 agricultural areas would have to be increased by 43 % (Ramankutty et al., 2008).

Deforestation can impact climate on local and global scales by changes in the energy, mass and momentum fluxes between the land surface and the atmosphere. Deforestation is frequently associated with $CO_2$ emissions, as the crops and marginal lands that usually take the place of trees after deforestation tend to hold less carbon per unit area than forests (Betts, 2000; Bala et al., 2007). The radiative forcing associated with an increase in atmospheric $CO_2$ is, from a climatic perspective, the most important biogeochemical impact of deforestation. Increases in $CO_2$ also have the potential to affect climate by altering transpiration rates, due to $CO_2$ fertilization reducing stomatal conductance and increasing leaf growth (Friedlingstein et al., 1999; Kleidon et al., 2000).





BGD
9, 14639–14687, 2012



The biogeophysical impacts of deforestation most pertinent to climate are changes to surface albedo, evapotranspiration and surface roughness length. Croplands and pastures tend to have higher albedo than forests, which causes them to absorb a smaller fraction of the incoming solar radiation. The roots of crops and grasses normally reach depths that are shallower than those of trees so that deforestation results in decreased evapotranspiration and a reduction in latent heat flux (Kleidon et al., 2000; Govindasamy et al., 2001; Bounoua et al., 2002; Bala et al., 2007). Evapotranspiration can also be reduced through the reduction in canopy capture following deforestation, as well as from reduced turbulence associated with a lower aerodynamic roughness length and colder temperatures. For large-scale land cover change the alterations in evapotranspiration can potentially impact cloud formation which can potentially impact atmospheric albedo and atmospheric longwave absorption.

In previous modelling efforts, the net temperature response to deforestation, to a large extent, is determined by the magnitudes of these opposing warming (higher atmospheric $CO_2$ and lower latent heat flux) and cooling (increased albedo) effects (for some examples: Bonan et al., 1992; Brovkin et al., 1999; Betts, 2000; Bonan, 2001; Matthews et al., 2004; Bala et al., 2007). The albedo-related cooling is particularly important at mid to high latitudes, where the presence of snow exacerbates the differences in reflectivity between forests and open lands (Betts, 2000; Bala et al., 2007), while the warming due to decreases in latent heat flux has a greater impact at low latitudes where the absolute changes in evapotranspiration are larger (Claussen et al., 2001; Bala et al., 2007).

Most modelling studies so far have analyzed the response to large-scale land cover change. In some, deforestation was global or performed over whole latitude bands (Bonan et al., 1992; Bonan, 2001; Bala et al., 2007; Bathiany et al., 2010; Davin and de Noblet-Ducoudre, 2010) while others simulated global historical anthropogenic deforestation (Matthews et al., 2004; Brovkin et al., 2006, 2009). In general terms, these past simulations show that the temperature response of high latitude deforestation is still dominated by the albedo effect, resulting in a cooler climate. That is, while the





BGD
9, 14639–14687, 2012



removal of trees causes atmospheric $CO_2$ concentrations to go up, the increase in albedo is enough to generate a reduction in surface air temperature (SAT) cooling. This cooling is global, and centered over the deforested areas (Claussen et al., 2001; Bala et al., 2007; Bathiany et al., 2010). Global temperature changes associated with mid latitude deforestation follow the general trend seen for high latitudes with a tendency for smaller temperature changes (Bala et al., 2007). Contrary to the cooling seen in the mid and high latitudes, simulated low latitude deforestation has resulted in a warmer climate, with the increase in temperature attributed to the reduction in evapotranspiration, and increased atmospheric $CO_2$, which dominates the temperature signal (Zhang et al., 2001; Davin and de Noblet-Ducoudre, 2010). Some studies have noted that a reduction in cloud cover, and hence reduced atmospheric albedo over deforested regions was an important contributor to the modelled warming (Bala et al., 2007). There have been indications from satellite based (Montenegro et al., 2009) and modelling (Pongratz et al., 2011; Arora and Montenegro, 2011) efforts that the temperature response is dependent on the scale and location of land cover change. According to these studies, in many high latitude and mid latitude areas deforestation would result not in cooling but in no significant change or net warming, with the $CO_2$ and evapotranspiration related warming overcoming the albedo induced cooling.

Here we use a global climate model of intermediate complexity, with a coupled carbon cycle model, to determine to what degree the scale of deforestation may influence the climate system's response to high, mid and low latitude deforestation. This is done by a series of experiments, where deforestation fractions range from 5 %–100 % of the tree covered area over these distinct latitude bands. The simulations are conducted from 2011 to 2200 with $CO_2$ emissions based on the IPCC A2 scenario.

## 2 Model description

The University of Victoria Earth System Climate Model (UVic ESCM) version 2.9 is an intermediate complexity climate model with horizontal resolution of





BGD
9, 14639–14687, 2012



1.8°(meridional) × 3.6°(zonal). It is composed of a vertically integrated energy-moisture balance atmospheric model, a dynamic-thermodynamic sea-ice model, a continental ice dynamics model, and version 2.2 of the Geophysical Fluid Dynamics Laboratory (GFDL) Modular Ocean Model (MOM2). The MOM2 is a general circulation ocean model with 19 vertical layers. The terrestrial carbon model is a modified version of the MOSES2 land surface model and the TRIFFID dynamic vegetation model (Cox, 2001; Cox et al., 2001). Ocean inorganic carbon is based on the OCMIP abiotic protocol. Ocean biology is simulated by an ecosystem model of nitrogen cycling (Oschlies and Garcon, 1999; Schmittner et al., 2005). Water, heat and carbon are conserved between model components with no flux adjustments. Cloud cover is set at a constant in the UVic ESCM. Bala et al. (2007) find that large-scale deforestation may influence cloud cover, and have an effect on the climate, however uncertainties exist in the change of cloud cover due to deforestation (Durieux et al., 2003; Chagnon et al., 2004; Montenegro et al., 2009). A full description of the atmospheric, oceanic, and sea ice models are in (Weaver et al., 2001), while the land surface scheme and dynamic vegetation model are described in (Cox, 2001; Cox et al., 2001).

### Vegetation model and land surface scheme

TRIFFID defines the state of the terrestrial biosphere in terms of soil carbon, and the structure and coverage of five plant functional types (PFT), broadleaf trees, needleleaf trees, $C_3$ grasses, $C_4$ grasses and shrubs within each grid cell (Cox, 2001). Using a carbon balance approach, TRIFFID determines the change in areal coverage, leaf area index and canopy height, as a result of net carbon fluxes calculated by the MOSES 2 land surface scheme. MOSES 2 recognizes the five PFTs used by TRIFFID, plus four non-vegetation types, bare soil, urban areas, land ice and inland water. Using the photosynthesis-stomatal conductance model developed by Cox et al. (1998), plant respiration and photosynthesis are dependant upon climate and atmospheric $CO_2$. Through this, the response of vegetation to climate occurs via climate-induced changes in the vegetation to atmospheric fluxes of carbon (Cox, 2001). In each 1.8° × 3.6° grid





BGD
9, 14639–14687, 2012



cell, the land coverage through time of PFTs is determined by a dynamic competition between the different PFTs. This is based on the Lotka-Volterra approach and a tree-shrub-grass dominance hierarchy. TRIFFID also allows agricultural areas to exist. These areas are defined as croplands and are treated as grass PFTs for determining their biogeochemical and biophysical behaviours. Soil carbon pools are increased through litterfall, and reduced by heterotrophic respiration. Litterfall is calculated as an area weighted sum from each PFT, and is dependant upon the degree of the land disturbance and competition between PFTs. Respiration is determined by the soil carbon content, a $Q_{10}$ soil temperature equation, and a piecewise linear soil moisture function, described in (Cox, 2001). Due to the Lotka-Volterra equations used for the competition algorithm, there exists a possibility for rapid loss of vegetation species if the land-use disturbance is large enough to trigger the requisite scenario. This scenario which can produce rapid increases or decreases in the abundance of a species is further explained in (Gotelli, 2001).

## 3 Experiments

For all experiments, the model is integrated from equilibrium at year 1800 to year 2000 forced by historical $CO_2$ emissions from combustion of fossil fuels and land-use change (Marland et al., 2002; Houghton, 2003). For the period between 2001 and 2100 simulations are forced by $CO_2$ emissions from the IPCC A2 scenario (Nakićenović and Swart, 2000) and from 2101 to 2200 $CO_2$ emissions are kept constant at the A2 scenario 2100 value.

Deforestation experiments cover the period between 2010 and 2200. Deforestation is simulated separately in three bands: the area northward of 40° N (high latitudes), the areas between 20° N to 40° N, and 20° S to 40° S (mid latitudes) and the area between 20° S to 20° N (low latitudes) (Fig. 1).

At the start of 2010, all experiments have the same crop area distribution based on Ramankutty and Foley (1999). The vegetation is specified by the DeFries and





BGD
9, 14639–14687, 2012



Townsend (1994) land cover data set. All results are compared to a control run where the crop area fraction remained fixed at the 2010 distribution. In the deforestation experiments crop area fraction is increased by different amounts in order to generate arbitrary deforestation ranging from 5 % to 100 % of the total forested area of the three different latitudes at 2010. The land cover change is performed in a single step at the start of 2011 by substituting trees with crops.

In all but the 100 % deforestation scenario only grid cells that contain both crops and forests are defined as eligible for deforestation (Fig. 2). In these simulations deforestation is performed by reducing the forest cover by a fixed amount in all eligible grid cells. The rationale is that experiments should simulate, as well as the coarse spatial scale of the model allows, land cover change resulting from an expansion in agriculture. In the 100 % scenario, any grid cell with forests was deemed eligible for deforestation. There is no 75 % deforestation simulation for the high latitudes, as the requirements for deforestation did not allow sufficient grid cells to be used to reach the required forest loss.

The expansion of croplands in the model follows a hierarchy where grasslands are converted to crops, before shrubs and trees. The result is that eligible grid cells that contain grasslands and shrubs prior to deforestation have these fractions converted to crops as well at the start of 2011. It should be noted that in TRIFFID crops and grasslands have identical biogeochemical and biogeophysical characteristics. The only difference is that grasslands can be outcompeted by other plant functional types while the crop distribution is prescribed. This means that all areas converted to crops in 2011 remain as such until the end of the experiments.

The use of an model of intermediate complexity in the study of deforestation has some drawbacks, among the more evident, the lack of a cloud response. Still due to computational and time constraints, the the large number of experiments required by the project could only be conducted with this kind of model.





BGD
9, 14639–14687, 2012



## 4 Results

After the initial disturbance forest cover is free to change. In presenting and discussing our results experiments are classified according to their initial arbitrary deforestation fraction. For example, the 5 % experiment refers to the simulation in which 5 % of the forest cover was removed instantaneously at the start of 2011.

### 4.1 Dieback

With the exception of the 100 % simulations, all deforestation scenarios, regardless of location, experience further loss of forests after the initial disturbance (Fig. 3). In all experiments, the fraction of forest loss of the 15 %–75 % simulations reaches a peak, and then tends to converge to around 50 % in the high latitudes, 70 % in the mid latitudes and 80 % in the low latitudes. No regrowth is seen in the 5 %–10 % scenarios, but the rate of forest loss slows down in the last half of the simulations.

In all cases, the post-deforestation dieback is caused by further forest loss in the deforested bins, which in the larger deforestation scenarios tend to lose all of their trees. It is this loss of trees in the deforested bins which produces the converging trend observed in the 15 %–75 % simulations, as their forest coverage in the deforested bins is near identical. The observed regrowth occurs in the non-deforested bins, where the forested fraction increases in relationship to the control for all simulations. This further loss of trees is not related to the dynamic vegetation model responding to climatic changes brought by deforestation but occurs because the response of the competition algorithms adopted by TRIFFID to the large and rapid land cover change implemented at 2011. Following the large land-use change, and subsequent changes to climate, TRIFFID's competition algorithm produced a continual loss of forests in the disturbed bins, with these forests being primarily replaced by shrubs. In that sense, the observed continuos loss of forest cover after deforestation are more akin to an external forcing to the simulations than to a response of the vegetation model to environmental change.





BGD
9, 14639–14687, 2012



### 4.2 Temperature and moisture response

#### 4.2.1 High latitudes

For all simulations deforestation causes a reduction in global SAT, with the cooling being proportional to deforested percentage (Fig. 4). The reduction in temperature is magnified at higher latitudes due to an increase in snow and ice cover and consequent increase in albedo. In the 100 % scenario the average temperature change from 20° N to 40° N was −0.42 K and the temperature change from 40° N and above was −0.78 K. Lower atmospheric $CO_2$ values are also responsible for some of the larger cooling seen in the 45 %–100 % deforestation simulations.

Deforestation also causes a decrease in global and local soil temperature (Fig. 5), however soil temperatures become warmer in areas with large forest cover prior to deforestation (Fig. 1). Soil temperatures show a similar trend to the SAT response, with the exception that the local (here defined as over deforested grid cells) soil temperatures of the 8 %–25 % simulations have positive soil temperature anomalies by 2200. There is a large drop in SATs and soil temperatures for all of the simulations around 2160. This decrease in temperature is due to a large change in the meridional overturning, resulting in a reduction of the oceanic poleward heat transport.

Although the global and local precipitation minus evaporation ($P-E$) trend is a drying, the local drying is of an order of magnitude larger than the global averages (Fig. 6). The areas with the largest drying occur in regions of increased soil temperatures. In these areas both evapotranspiration and precipitation increase, however the increase in evapotranspiration is larger than the increase in precipitation due to the enhanced soil temperatures. In the areas where conditions become wetter, there is also an increase of both precipitation and evapotranspiration, however the increase in precipitation is larger. For all simulations deforestation results in an overall drier climate over deforested areas (Fig. 6).





BGD
9, 14639–14687, 2012



### 4.2.2 Mid latitudes

The initial mean global SAT response is warming, followed by a decrease in the positive anomalies so that by the end of the simulation all deforestation scenarios have lower global SATs than the control (Fig. 7). Positive anomalies are small and last only a few years in the lesser deforestation fractions. The 9 % and 10 % scenarios have SATs very close to the control up to the end of the 21st century. Positive anomalies are larger (up to ∼ 0.4 K) in the 15 %–25 % scenarios and SATs remain above the control values until about 2140. The 45 %–100 % scenarios exhibit the largest deviations from the control, with both positive and negative anomalies proportional to the deforestation fraction. Positive anomalies decrease rapidly in the 75 % and 100 % cases, where SATs are already colder than the control by 2040. In all of the simulations, the largest SAT reductions occur over deforested areas. Due to the increase in local albedo, deforested areas remain colder than the control even during periods where higher atmospheric $CO_2$ concentrations cause mean global positive SAT anomalies (Fig. 7).

The global soil temperature response shows a similar pattern to the SATs, however the 15 %–25 % simulations remain warmer for the duration of the experiment (Fig. 8). In all simulations, average local soil temperatures over deforested areas are warmer than those of the control, with cooling occurring outside of the deforested areas (Fig. 8). The initial local soil temperature response is proportional to the amount of deforestation. In most cases positive anomalies continue to increase, the exceptions being the 75 % and 100 % simulations which, due to reduced rates of energy absorption, resulting from increased albedo and outgoing latent heat flux, have a decreasing trend following deforestation. This is followed by an eventual increase, so that by the end of the simulations the 75 % and 100 % local soil temperature anomalies are similar to those seen in the 15 %–50 % simulations.

Similar to the high latitudes, meridional overturning slows around 2160 in all of the simulations, except the 15 % and 25 % simulations. In the 15 % and 25 % simulations,





BGD
9, 14639–14687, 2012



the slight differences in climate compared to the other simulations, was enough to prevent this change in meridional overturning.

In all scenarios, deforestation leads to mean drying over land, with the decrease in moisture driven predominately by change over deforested bins (Fig. 9). Drying over deforested areas tends to be proportional to the deforestation fraction, the exception being the 100 % simulation which, although drier than the control, has higher $P-E$ values than the 75 % scenario.

Mean evapotranspiration and precipitation both increase over deforested areas, however in all simulations evapotranspiration increases more than precipitation. Differing from the mean response, conditions are wetter in a significant number of deforested bins over Eastern Asia (Fig. 9). While precipitation does increase, the positive $P-E$ anomaly over these deforested bins is caused by a decrease in evapotranspiration. The change in soil temperature over deforested areas in Eastern Asia also tends to be different from that of other areas. While the general response is warming, the temperature increase tends to be smaller and many bins in the area show cooler soil conditions after deforestation (Fig. 8).

#### 4.2.3 Low latitudes

The global SAT response to deforestation for all simulations is a general increase followed by cooling. The magnitude and rate of initial warming tends to be proportional to the deforested area fraction and higher deforestation fractions tend to reach their peak positive anomaly sooner, although similar to the high and mid laitutde simulations, by 2200 all scenarios produce colder SATs (Fig. 10). The SAT change over deforested bins differs significantly from what is seen globally. When the deforestation fraction is 10 % or lower, SAT anomalies over deforested bins are negative for the duration of the experiment, with larger anomalies occurring over the 22nd century. Deforestation fractions of 15 % and above result in initial warming, but by about 2080 SATs over these deforested bins start to exhibit negative anomalies (Fig. 10). Throughout the simulations the





BGD
9, 14639–14687, 2012



colder SATs spread radially outward from the deforested areas, eventually resulting in lower values across the globe at the end of the experiments (Fig. 10).

The global soil temperature response to deforestation exhibit a pattern similar to that of the global SAT with the difference that the soil temperature anomalies are always positive (Fig. 11). The pattern of local soil temperature response over deforested bins is similar to the global response for the 5 %–50 % simulations. The 75 % and 100 % scenarios, similarly to what is observed at mid latitudes, show positive anomalies that decrease during to 21st century resulting in soil temperatures that are still higher than the control but lower than those observed in the 15 %–50 % simulations.

The low latitudes also experienced some changes to meridional overturning, however this only occurred in the 50 % and 100 % simulations. In a process similar to the mid latitudes, the 50 % and 100 % scenarios had enough of a change to the climate to produce this change in overturning.

The global moisture response over land of the low latitudes is less consistent between simulations than that of the high and mid latitude simulations, with most deforestation fractions changing between drier and wetter conditions during the experiment (Fig. 12). During the last 20 yr, all experiments exhibit negative $P-E$ anomalies. Drying is more intense and starts earlier in experiments with deforestation fraction above 25 %.

In all experiments, conditions become drier over deforested bins and the $P-E$ anomalies over these areas are an order of magnitude larger than those registered in the global response (Fig. 12). Both evapotranspiration and precipitation increase over deforested bins and drying occurs because the increase in evapotranspiration overtakes the increase in precipitation. It is interesting to note that the local drying is usually more intense in the mid latitudes than in the low latitude simulations.

While the mean local response is drying, some areas in equatorial Africa and the Amazon become wetter after deforestation. Contrary to the areas that become wetter in the mid latitudes simulations, the positive $P-E$ anomalies in the low latitude deforested bins are caused by an increase in precipitation and not decreased evapotranspiration.





BGD
9, 14639–14687, 2012



Compared to the mid latitudes, where the wetter conditions occur in areas of mixed warming and cooling soil temperatures, low latitude bins with positive $P-E$ show no significant variation in soil temperature (Fig. 11). From (Fig. 12) it can be seen that there is an increase in $P-E$ outside the deforested areas, which is consistent for all simulations. It is this increase in moisture in non-deforested areas, as well as the less pronounced decrease in moisture in the deforested areas for the 5 %–50 % simulations, that leads to an average global increase of moisture over land at various times in the simulations for the 7 %–50 % scenarios.

### 4.3 Carbon cycle

#### 4.3.1 High latitudes

All deforestation simulations show an initial increase in atmospheric $CO_2$ relative to the control. The increase is proportional to deforested area and ranges from 3.03 to 50.40 ppmv (Fig. 13). This expected increase in $CO_2$ concentration is due to the release of carbon stored in the forests (Forster et al., 2007; Friedlingstein and Prentice, 2010). Although the relative difference between the simulations and the control decreases in the first 10 yr after deforestation, atmospheric $CO_2$ values for the 8 %–25 % deforestation experiments remain above those of the control during the whole simulation due to continued, competition algorithm induced, loss of forests leading to increased $CO_2$ emissions.

As simulations progress however, the other scenarios exhibit periods when atmospheric $CO_2$ concentrations are lower than those of the control (Fig. 13). Reduction in $CO_2$ concentrations are seen in the 5 %–7 %, and 45 %–100 % deforestation experiments. The $CO_2$ decreases in the 5 %–7 % deforestation scenarios are small and by the end of the simulation these experiments have $CO_2$ concentrations slightly larger than the control. In the 45 %–100 % deforestation scenarios atmospheric $CO_2$ values are lower than those of the control from around year 2040 to the end of the simulations.





BGD
9, 14639–14687, 2012



In all simulations the behaviour of ocean carbon is similar to atmospheric $CO_2$ and all simulations with a relative loss of atmospheric $CO_2$ also show a relative reduction in ocean carbon (Fig. 14).

Atmospheric carbon closely mirrors the changes to land carbon. $CO_2$ levels are higher in experiments where deforestation leads to net loss of carbon by land and lower in simulations where the removal of trees cause an increase in land carbon stocks (Fig. 14). Deforestation always results in an decrease in vegetation carbon and an increase in soil carbon. The net change in land carbon, and consequently the atmospheric $CO_2$ response, is determined by the relative magnitude of these soil and vegetation carbon changes.

Ignoring the small drawdowns of the 5 %–7 % experiments, deforestation of up to 25 % results in loss of land carbon and increase in atmospheric carbon (Fig. 14). For the 45 %–100 % deforestation scenarios the increase in soil carbon overcomes the losses from vegetation carbon. In these simulations the land gains carbon at the expense of the atmosphere, where $CO_2$ concentrations decrease (Fig. 14).

The increase in soil carbon is related to a reduction in soil heterotrophic respiration due to colder and drier conditions and also to an increase in modelled net primary productivity (NPP) over deforested areas. In the 5 %–25 % simulations the increase in soil carbon was larger in the non-deforested areas than in the deforested areas. We take this as an indication that climate played a larger role than alterations in NPP due to land cover change in the increase of soil carbon in these experiments. Deforested areas contribute to approximately 58 %–70 % of the increase in soil carbon in the 45 %–100 % deforestation scenarios, showing that in these experiments the higher NPP of croplands also played a role in accumulation of land carbon. Although croplands are usually associated with reductions in NPP, observations have found an increase in NPP after forest loss in high latitudes (Roy et al., 2001), and modelling efforts have found an increase due to higher grassland productivity and $CO_2$-fertilization despite colder temperatures (Bathiany et al., 2010).





BGD
9, 14639–14687, 2012



### 4.3.2 Mid latitudes

In all scenarios, deforestation produces a rapid increase in atmospheric $CO_2$ (2.65 to 47.58 ppmv) as the carbon lost by vegetation due to deforestation makes its way into the atmosphere (Figs. 13, 14). This is followed again, in all scenarios, by a decrease in $CO_2$ values. After this initial pulse, the behaviour of the simulations differs. The 5 %–25 % scenarios see increases relative to the initial pulse ranging from 22 %–235 % by 2200, with the 15 % scenario having the largest increase. The 45 %–100 % scenarios do not experience an increase in $CO_2$ relative to the initial pulse, exhibiting instead reductions ranging from 33 %–99 % by 2200, with the 75 % scenario showing the largest decrease. This caused the 75 % simulation to exhibit atmospheric $CO_2$ concentrations very similar to those of the control experiment during the last 50 yr of the simulation.

All simulations experience a global increase in soil carbon that offsets a portion of the losses in land carbon caused by deforestation and dieback. Following a brief (about four years) initial decrease in soil carbon, all experiments show a relatively rapid increase of this property up to about 2040 to 2060. The magnitude of the increase is dependent on the deforestation fraction and in all experiments this is accompanied by a reduction in atmospheric carbon (Fig. 14). In the lowest (5 %–7 %) and highest (45 %–100 %) deforestation fractions this increase is followed by a period where soil carbon stocks remain stable or continue to increase at slower rates. In the 15 %–25 % experiments soil carbon decreases from about 2040 until the end of the simulation but the reduction is not enough to cause negative soil carbon anomalies.

A transition occurs between the 15 %–75 % simulations where the increase in soil carbon becomes larger than the increase in atmospheric carbon, however only the 75 % simulation experienced a large enough increase in soil carbon to produce an atmospheric carbon reduction relative to the control (Figs. 13, 14). The 15 % simulation has the largest difference between atmospheric carbon and soil carbon (55 Pg C), this difference decreases with increases in the deforested area fraction, resulting in a switch in the 50 % simulation, where the soil carbon increase is once again larger than the





BGD
9, 14639–14687, 2012



atmospheric carbon increase. The large loss in atmospheric carbon seen in the 75 % simulation relative to the 50 % simulation is almost completely compensated by a gain in soil carbon. Although the 75 % simulation had a reduction in atmospheric $CO_2$, it did not experience the increase in land carbon, which occurred in the high latitudes for simulations with a reduction of atmospheric $CO_2$.

For all experiments, both forested and non-forested bins contribute to the initial increase in soil carbon. Due to changes in climate and enhanced NPP caused by increased $CO_2$ Sitch et al. (2008), non-deforested bins maintain positive soil carbon anomalies over the duration of all experiments. As simulations progress, some scenarios experience eventual reductions in soil carbon, associated with loss of carbon in deforested bins. These losses are larger for the 15 %–25 % scenarios, (Fig. 14) and are associated with increased respiration, due to warmer soil temperatures (Fig. 8) and wetter conditions over their deforested bins when compared to those of the other scenarios (Figs. 6, 9, 12). The increase in NPP, as well as the enhanced drying and cooler temperatures over the deforested bins of the 75 % and 100 % experiments causes these areas to gain soil carbon continuously during the experiments and at the simulations' end, there is more soil carbon in the deforested areas of the 75 % and 100 % scenarios (~ 53 % and 62 % of the total respectively) than in all non-deforested bins. The large increase of soil carbon in the higher deforestation fraction experiments leads to the larger atmospheric $CO_2$ drawdown seen in these scenarios.

Ocean carbon stocks are responding to atmospheric $CO_2$ (Fig. 14) as ocean carbon increases and decreases with the fluctuating $CO_2$ values.

#### 4.3.3 Low latitudes

As in the high, and mid latitudes, for all low latitude simulations, the carbon lost by vegetation due to deforestation enters the atmosphere, generating a rapid increase in $CO_2$ concentrations proportional to the extent of deforestation (7.16 to 127.12 ppmv). Due to the larger quantity of trees removed in the low latitudes, this initial $CO_2$ increase is higher than what is seen in the high and mid latitudes combined (Fig. 13) and the low





BGD
9, 14639–14687, 2012



latitudes are the only set of experiments where negative atmospheric $CO_2$ anomalies do not occur.

This increase is followed by a period of diminishing $CO_2$, with the rate of decrease proportional to the deforestation fraction. Atmospheric $CO_2$ values in the 75 % and 100 % scenarios fall relatively quickly, and for the duration of the experiments, remains below those of the initial pulse. This is not the case for all other scenarios, where by no later than the mid 21st century, the atmosphere holds more carbon than what was lost initially by vegetation due to deforestation (Fig. 13). Around the mid 22nd century all experiments start to show a negative trend in $CO_2$ concentrations.

The change in $CO_2$ concentrations at 2200 relative to the initial pulse of $CO_2$ is much larger in the low latitudes than the high or mid latitudes due to a larger land-use change. The 5 %–45 % simulations all have an increase of $CO_2$ at 2200 relative to the initial pulse. This increase ranges from 6 % to more than five times the post-deforestation pulse concentration, with the largest increase occurring in the 7 % scenario. The 50 %–100 % simulations had a decrease in $CO_2$ by 2200 relative to the initial pulse, ranging from 10 %–65 % with the 100 % scenario producing the largest decrease.

The low latitudes had the same initial soil carbon response to deforestation as the high and mid latitudes, with a small initial decrease over the first three to four years followed by a relatively fast increase (Fig. 14). As with the mid latitudes, the changes in soil carbon are explained by continuous increase in carbon density over non-deforested areas and a mixed response in the deforested bins. The largest soil carbon losses occur in the intermediary deforestation fractions, where soils are warmer and not as dry. Different from the high and mid latitudes, these losses resulted in periods where some intermediary fractions, like the 25 % scenario, exhibited negative global soil anomalies in relationship to the control. Again as seen in the high and mid latitudes, the experiments with the smaller soil carbon anomalies are the ones which show the largest atmospheric $CO_2$. Increases in NPP, relatively colder temperatures and drier conditions lead to large soil carbon gains by deforested bins in the higher fraction deforestation





BGD
9, 14639–14687, 2012



scenarios. Similarly to the mid latitudes, the deforested bins of the 75 % and 100 % simulations hold the majority of the global soil carbon by the end of the experiments.

The ocean carbon response to low latitude deforestation is very similar to the high and mid latitudes, where ocean carbon to a certain degree mirrors atmospheric carbon. In the low latitudes we do not see the same level of post initial pulse reduction in atmospheric carbon as was observed in the high and mid latitudes, and the ocean carbon also shows this, as there is less variation in total ocean carbon between the simulations, due to the oceans slower response to atmospheric carbon change (Fig. 14).

## 5 Discussion

### 5.1 High latitudes

The lower temperatures observed in our 5 %–25 % deforestation experiments are in agreement with previous modelling studies where the albedo effect outweighs the increase in $CO_2$ for high latitude deforestation (Claussen et al., 2001; Bala et al., 2007; Bathiany et al., 2010). Differently from these earlier results, our cooling is magnified in the 45 %–100 % scenarios by a decrease in atmospheric $CO_2$ caused largely by an accumulation of soil carbon over deforested areas. By 2100 our 100 % simulation produced cooling of approximately 0.4 K, with an average cooling over the duration of the simulation of 0.329 K. The average cooling is similar to what was found by Bathiany et al. (2010), where a cooling of 0.25 K is observed, however our cooling at 2100 is only half of what is modelled by (Bala et al., 2007). Bala et al. (2007) produced a smaller albedo change than what was seen in our simulations, albedo increased by 2.02 % to 12.74 % by 2100 in the high latitudes, with larger deforestation events producing higher increases of albedo, compared to 10.7 % increase of high latitude albedo by 2100 in the study by Bala et al. (2007). Bathiany et al. (2010) produced a larger albedo change than our simulations, with an average increase of 0.070, compared to our average increase of 0.0065 to 0.0404. Due to the differences in selected latitude range, as well





BGD
9, 14639–14687, 2012



as the differences in model components and emissions, it is difficult to pinpoint which discrepancies in these studies produce the variation in temperatures.

Complete deforestation of areas above 45° N caused an increase in soil carbon over deforested areas in simulations conducted by Bathiany et al. (2010). In their case the extra soil carbon was not enough to compensate for the loss of biomass and litter carbon, leading to an overall loss of land carbon and a relatively small ($\leq 5$ ppm) increase in atmospheric $CO_2$. While no information on soil carbon is reported by Bala et al. (2007), these authors find a similar (5 ppm at 2100) increase in atmospheric $CO_2$ in their 100 % high latitude deforestation experiments. The Bathiany et al. (2010) experiments did not account for anthropogenic emissions, which are considered by the Bala et al. (2007) experiments.

In a managed forest, clear cutting reduced soil carbon (Diochon et al., 2009). Analyzing conditions 100 yr after land cover change Poeplau et al. (2011) conclude that the conversion of forests to cropland in temperate zones results in about a 32 % ± 20 % decrease in soil carbon. The same authors note that the conversion of grassland to forest tend to cause a soil carbon *reduction* of about 7 % ± 23 %. Even our low end deforestation scenarios result in land cover change at much larger spatial scale than those analyzed by the observational studies and comparison between our results should be made with caution.

Starting at around 2110, the 15 %–50 % experiments all present similar forest loss fractions (Fig. 3), an indication that the separation of scenarios which cause net land carbon loss ($\leq 25$ %) from those resulting in net land carbon gain ($\geq 45$ %) is not a simple function of total deforested area but also dependent on the initial amount of land cover change.

The initial surface air and soil cooling of the 45 %–100 % experiments are markedly larger (Figs. 4, 5) than those of the other simulations. It is this rapid albedo-related cooling, and the associated slow-down of soil respiration, which lead to the larger retention of carbon over land in these scenarios. As the surface albedo and atmospheric $CO_2$ begin to change, it influences the surface energy balance, which in turn effects





BGD
9, 14639–14687, 2012



the soil temperatures. In the case of the high latitudes, the resultant magnitude of the changes to the energy balance that lead to the decrease in soil temperatures.

Removal of trees shortens the roughness length and causes a reduction in outgoing sensible heat flux, a warming effect, over deforested bins. At the same time, deforested areas experience increases in the outgoing latent heat flux, and net surface radiation. The final result is a reduction in net incoming energy and soil cooling (Fig. 15). This is a similar effect to the temperature reduction mechanism described in (Lee et al., 2011), where it was found that in the high latitudes, temperatures decreased despite a decreased outgoing sensible heat flux.

The energy budget is balanced by the equation:

$$R_n = \mathrm{LE} + H + G \quad (1)$$

where $R_n$ is the net surface radiation, LE is latent heat, $H$ is sensible heat, and $G$ is the ground heat flux. By increasing the surface albedo, and latent heat, the decreased surface skin temperature contributes to the reduced soil temperatures.

The reduction in soil moisture, while less important in explaining the initial accumulation of soil carbon, is likely exerting a larger influence after about 2060, when soil carbon continues to increase (albeit at slower rates) in spite of increasing soil temperature over deforested areas (Figs. 5, 14). In Fig. 6, an interesting result is shown where the drying in the 100 % simulation is not the largest, compared to the temperature and carbon response, where the 100 % scenario produces the most extreme changes. The increased moisture is likely due to the larger area used for 100 % deforestation, with more snow covered areas and more cooling resulting in less evapotranspiration. This result can also be observed in (Fig. 15) where the latent heat flux of the 100 % simulation is less than the 45 % and 50 % scenarios for the majority of the simulation.

Evidently, we do not make the claim that our findings justify large scale high latitude deforestation as a means of carbon sequestration. Nevertheless, our results point to the complex interaction between soil carbon dynamics and climate and the significant role this interaction plays on the modelled climatic response to land cover change. Given





BGD
9, 14639–14687, 2012



the large uncertainties associated with the modelled terrestrial carbon cycle (Friedlingstein et al., 2006), our results also point to the need for greater understanding of how organic matter behaves in soils (Schmidt et al., 2011) and for the adoption of this new knowledge by terrestrial models.

### 5.2 Mid latitudes

The SAT cooling seen in the 100 % mid latitude deforestation scenario is in general agreement with the studies by Bala et al. (2007); Davin and de Noblet-Ducoudre (2010), albeit the reduction in temperature at 2100 produced by our experiment (−0.077 K) is larger than the one described by Bala et al. (2007) (−0.04 K). Our simulations produced fairly similar albedo changes to Bala et al. (2007) who found albedo increases of 5.0 % and 4.7 % in the mid latitudes, compared to our 1.32 % to 4.76 % albedo increase. Also in agreement, our mid latitude cooling is smaller than what was seen in previous modelled high latitude deforestation (Bala et al., 2007; Davin and de Noblet-Ducoudre, 2010, Fig. 7). The Davin and de Noblet-Ducoudre (2010) simulations involved a more drastic deforestation event with a completely forested world converted to a completely deforested world, and constant $CO_2$ values, however our local and global response, although lesser in magnitude, is a cooling as well, due to the albedo effect.

By 2100 the 75 % scenario has near identical forest loss as the 25 %–50 %. However, the the 75 % scenario, similar to the 100 % scenario, shows a higher initial albedo increase, as well as reduced atmospheric $CO_2$ through increased soil carbon, driving further global cooling. The rapid increase in albedo in the 75 % and 100 % scenarios effect the soil temperatures as well, which decrease over the first 60 yr, before the temperature anomalies begin to trend upwards again. This points to the importance of the magnitude of the initial disturbance on modelled climates. Although the 15 %–75 % scenarios all reach similar forest loss by 2200, and display converging albedo values, the larger initial land use change results in higher initial albedo values which allow





BGD
9, 14639–14687, 2012



the 45 %–75 % simulations to reach lower temperatures despite having final land use change fractions similar to the 15 %–25 % simulations.

In the mid latitudes, the local response to deforestation differs compared to the high latitudes. The increase in evapotranspiration leads to more drying than what is observed in the high latitudes (Figs. 6, 9, 15, 16). This is also accompanied by increased soil temperatures in the mid latitude deforested bins, opposed to the local response to high latitude deforestation (Figs. 5, 8). Soil temperatures increase, despite the added cooling from increased modelled outgoing latent heat and albedo, primarily due to the decreased roughness length following deforestation. Decreased roughness lengths lead to less outgoing sensible heat, which becomes the dominant driver in local soil temperatures for these experiments. Following deforestation the outgoing sensible heat flux (Fig. 16) decreases more than at the high latitudes, resulting in a higher retention of heat in the soils, and thus higher soil temperatures.

Sensible heat flux in the UVic ESCM is represented by:

$$\mathrm{SH} = \rho C_\mathrm{D} U (T_\mathrm{s} - T_\mathrm{a}) \tag{2}$$

where SH is sensible heat, $\rho$ is the density of air, $U$ is the wind speed, $T_\mathrm{s}$ is the soil temperature, $T_\mathrm{a}$ is the SAT and $C_\mathrm{D}$ is the Dalton number given by:

$$C_\mathrm{D} = \mathrm{k}^2 (\ln \frac{z}{z_0})^{-1} (\ln \frac{z}{e^{-2} z_0})^{-1} \tag{3}$$

where k is the Von Karman constant, $z$ is a reference height and $z_0$ is the aerodynamic roughness length (Meissner et al., 2003; Matthews et al., 2004) .

In the simulations, deforestation reduces $C_\mathrm{D}$ because the grassland $z_0$ is smaller than the forest $z_0$. This change in $C_\mathrm{D}$ is what inevitably reduces SH, as the other terms in the equation act towards increasing SH. Decreasing roughness length over the mid latitude deforested bins reduces the surface's ability to lose sensible heat, resulting in a net soil temperature increase over these areas.

The accumulation of global soil carbon is driven by the increase in NPP and a decrease in soil respiration. The change in soil carbon accumulation is intrinsically tied to





BGD
9, 14639–14687, 2012



the change in soil temperature and moisture. Globally, all deforestation fractions led to drier conditions over land, and global soil temperatures tend to decrease, the exception being the 15 %–25 % scenarios (Figs. 9, 8).

The opposing effects of warming and drying trends determines the exchange of carbon between soil and atmosphere. The 15 %–25 % scenarios experience the largest local warming (as well as being the only experiments to have globally warmer soil temperatures by 2200) however do not experience the same level of drying as is seen in the 45 %–100 % scenarios. The 45 %–100 % scenarios also experience less warming then the 15 %–25 % scenarios, leading to reduced respiration in the 45 %–100 % cases and larger drawdown of atmospheric $CO_2$. This results in larger soil carbon quantities and less atmospheric $CO_2$ (Figs. 13, 14). The increase in $CO_2$ seen in the 5 %–25 % simulations is linked to the less rapid loss of forests than was seen in the 45 %–100 % scenarios, resulting in less albedo cooling, and a slower release of $CO_2$ over time. The warmer global soil temperatures of the 15 %–25 % scenarios are due to the higher surface air temperatures, where increased $CO_2$ concentrations, as well as lower surface albedos than the 45 %–100 % scenarios, highlighting the complex interactions which take place in determining local and global temperatures.

Similar to the high latitudes, some mid latitude deforestation simulations differed from observations by Diochon et al. (2009); Nave et al. (2010) where deforestation led to a decrease in soil carbon due to increased respiration. In our experiments the 45 %–100 % simulations resulted in a local soil carbon increase, which is in agreement with observations by Poeplau et al. (2011) where the conversion of grassland to forest causes a soil carbon reduction.

The response to deforestation in the mid latitudes shows the transition between high and low latitude deforestation where albedo change becomes a less dominant driver of temperature and changes to $CO_2$ concentrations and the sensible heat flux plays a larger role in local and global temperature response. The high latitudes experience cooling in every simulation almost instantaneously (Fig. 4), whereas the presence of higher $CO_2$, and decreased outgoing sensible heat flux overcome the albedo change





BGD
9, 14639–14687, 2012



and increased latent heat, resulting in longer lasting warmer conditions in the mid latitudes (Fig. 7).

### 5.3 Low latitudes

The initial air surface warming which occurs due to low latitude deforestation is in agreement with the studies by Shukla et al. (1990); Bala et al. (2007); Bathiany et al. (2010). The magnitude of the temperature change is not as consistent with previous studies due to differences in the location and magnitude of deforested areas and $CO_2$ concentrations. Bala et al. (2007) observed a global warming of 0.7 K by 2100, and Bathiany et al. (2010) an average warming of 0.4 K over their 300 yr study. Their simulations removed all trees in the low latitudes, whereas our 100 % simulation resulted in a 0.044 K warming by 2100 and an average warming of 0.042 K. Our albedo increase was larger than the albedo increase seen by Bala et al. (2007), who found an albedo increase in the low latitudes of 4.1 %, compared to our 2.95 % to 10.78 % increase in albedo by 2100. However our average albedo increase was smaller than the albedo increase reported by Bathiany et al. (2010) who found an average surface albedo increase of 0.042 compared to our range of 0.01 to 0.02. The local cooling observed in our study is seen, although not to the same extent in some (Bala et al., 2007; Claussen et al., 2001) but not all (Bathiany et al., 2010) comparable experiments.

The difference between these studies is likely due to the different carbon and albedo responses, as well as some of the inherent differences in the models used. By 2150 our 100 % scenario had an increased $CO_2$ concentration of $\sim$ 66.5 ppm, compared to the Bala et al. (2007) study with a $CO_2$ increase of 299 ppm. Another difference is that the Bala et al. (2007); Bathiany et al. (2010) studies produced a reduction in evapotranspiration, as well as a decreased atmospheric albedo from reduced cloud cover, both of which contribute to increased temperatures.

Satellite based studies show that that depending upon the scale of deforestation, cloud cover may not change and may even increase over disturbed areas (Durieux et al., 2003; Chagnon et al., 2004; Montenegro et al., 2009). This contradicts the results





BGD
9, 14639–14687, 2012



of Bala et al. (2007); Bathiany et al. (2010) and may lead to added cooling not accounted for in these modelling studies. Bala et al. (2007) found that the net albedo change over the deforested regions was negligible as the increase in surface albedo was compensated by the decrease in atmospheric albedo, and suggests that cloud cover may play a major role in tropical climates.

Clouds cover is prescribed in the UVic ESCM and in our experiments the post-deforestation surface albedo increase is not compensated by a decrease in atmospheric albedo due to a reduction in cloud cover over deforested areas. This helps explains the local cooling registered by our simulations and lends support to the argument that a reduction in cloud cover is an important component of the modelled temperature response to deforestation in the tropics see in previous experiments.

Bathiany et al. (2010) report that low latitude deforestation causes a decrease in modelled total land carbon, and the same occurs in all of our simulations (Fig. 14). The same authors also see a reduction in soil carbon in the deforested areas, and increases in the non-deforested areas, which is observed in our 5 %–45 % scenarios. Our 50 %–100 % soil carbon responses do not match the results of Bathiany et al. (2010) as we see an increase in soil carbon in all locations, regardless of land cover change. Soil temperatures were larger in the low latitudes, and conditions were wetter than the mid latitudes. It is likely this difference in climate that causes the larger reduction in local soil carbon, in the 5 %–45 % scenarios than the mid latitude cases. During the first 100 yr of the simulations the 5 %–25 % scenarios become wetter, relative to their initial drying following deforestation (Fig. 12). This change in behaviour, as well as warmer soil temperatures (Fig. 11), can account for the increased respiration relative to carbon drawdown, and hence the decreased local soil carbon in these experiments.

Local soil warming occurs due to the same energy balance modifications seen in the mid latitudes, with higher temperatures related to a decrease in outgoing sensible heat flux that overcomes the increase in outgoing net radiative and latent heat fluxes (Fig. 17). The higher local soil temperature anomalies present in the low latitudes, occur due to the larger reductions in outgoing sensible heat, as well as increased rates





BGD
9, 14639–14687, 2012



of change in the energy budget of the soils, than what is seen in the mid latitudes (Figs. 16, 17). The increase in outgoing latent heat flux and reduction in sensible heat flux, also explains the lower SATs over deforested areas in the low latitudes (Fig. 10).

The direction of the soil carbon response of our 5–45 % low latitude simulations are in agreement with observations by Diochon et al. (2009); Nave et al. (2010) but differ from what is described by Poeplau et al. (2011). Although NPP increases due to the forest-to-cropland conversion, this is not enough to overcome the changes in respiration, where consistently higher soil temperatures, as well as less drying than is observed in the mid latitudes (Figs. 8, 11, 9, 12), lead to a larger reduction in local soil carbon. However our 50 %–100 % simulations present the same response as our high and mid latitude results, where local soil carbon increases. This highlights the importance of the initial magnitude of land use change, and resultant climate change, on the soil carbon response to deforestation in the UVic ESCM. The 15 %–75 % simulations all have converging levels of forest loss by 2120 (Fig. 3), thus the rate of change of land cover can also play a role in soil carbon retention. This further enhances the argument that the change in soil carbon arrises through a multitude of pathways, which influence the influx and outflux of carbon.

The increase in atmospheric $CO_2$, and warmer temperatures seen in our low latitude simulations, are climatic effects more often associated with modelled deforestation. Even then, due mostly to the soil carbon response, $CO_2$ and temperature increases are not proportional to deforested area. Seeing as how the location and scale of deforestation can lead to either an increase or decrease to local and global soil carbon, our results call attention to the subtleties of this response and toward a need for a better understanding the complexity of soil carbon dynamics (Schmidt et al., 2011).

*Acknowledgements.* The authors are grateful for funding provided by the NSERC-CREATE program, NSERC, AIF and ACEnet.





BGD
9, 14639–14687, 2012



## References


Arora, V. and Montenegro, A.: Small Temperature benefits provided by realistic afforestation projects, Nat. Geosci., 4, 514–518, 2011. 14643

Bala, G., Caldeira, K., Wickett, M., Phillips, T. J., Lobell, D. B., Delire, C., and Mirin, A.: Combined climate and carbon-cycle effects of large-scale deforestation, P. Natl. Acad. Sci. USA, 104, 6550–6555, 2007. 14641, 14642, 14643, 14644, 14657, 14658, 14660, 14663, 14664

Bathiany, S., Claussen, M., Brovkin, V., Raddatz, T., and Gayler, V.: Combined biogeophysical and biogeochemical effects of large-scale forest cover changes in the MPI earth system model, Biogeosciences, 7, 1383–1399, doi:10.5194/bg-7-1383-2010, 2010. 14642, 14643, 14653, 14657, 14658, 14663, 14664

Betts, R.: Offset of the potential carbon sink from boreal forestation by decreases in surface albedo, Nature, 408, 187–190, 2000. 14641, 14642

Bonan, G.: Observational evidence for reduction of daily maximum temperature by croplands in the Midwest United States, J. Climate, 14, 2430–2442, 2001. 14642

Bonan, G., Pollard, D., and Thompson, S.: Effects of boreal forest vegetation on global climate, Nature, 359, 716–718, 1992. 14642

Bounoua, L., DeFries, R., Collatz, G., Sellers, P., and Khan, H.: Effects of land cover conversion on surface climate, Clim. Change, 52, 29–64, 2002. 14642

Brovkin, V., Ganopolski, A., Claussen, M., Kubatzki, C., and Petoukhov, V.: Modelling climate response to historical land cover change, Global Ecol. Biogeogr., 8, 509–517, 1999. 14642

Brovkin, V., Claussen, M., Driesschaert, E., Fichefet, T., Kicklighter, D., Loutre, M., Matthews, H., Ramankutty, N., Schaeffer, M., and Sokolov, A.: Biogeophysical effects of historical land cover changes simulated by six Earth system models of intermediate complexity, Clim. Dynam., 26, 587–600, 2006. 14642

Brovkin, V., Raddatz, T., Reick, C. H., Claussen, M., and Gayler, V.: Global biogeophysical interactions between forest and climate, Geophys. Res. Lett., 36, L07405, doi:10.1029/2009GL037543, 2009. 14642

Butler, R.: The Amazon: The World's Largest Rainforest, available at: http://rainforests.mongabay.com/amazon, 2006. 14641

Chagnon, F., Bras, R., and Wang, J.: Climatic shift in patterns of shallow clouds over the Amazon, Geophys. Res. Lett., 31, L24212, doi:10.1029/2004GL021188, 2004. 14644, 14663






BGD
9, 14639–14687, 2012



Claussen, M., Brovkin, V., and Ganopolski, A.: Biogeophysical versus biogeochemical feedbacks of large-scale land cover change, Geophys. Res. Lett., 28, 1011–1014, 2001. 14642, 14643, 14657, 14663

Cox, P.: Description of the "TRIFFID" Dynamic Global Vegetation Model, Hadley Centre Technical Note, 24, 1–17, 2001. 14644, 14645

Cox, P., Huntingford, C., and Harding, R.: A canopy conductance and photosynthesis model for use in a GCM land surface scheme, J. Hydrol., 213, 79–94, 1998. 14644

Cox, P. M., Betts, R. A., Jones, C. D., Spall, S. A., and J., T. I.: Modelling Vegetation and the Carbon Cycle as Interactive Elements of the Climate System, Hadley Centre Technical Note, 23, 1–29, 2001. 14644

Davin, E. L. and de Noblet-Ducoudre, N.: Climatic impact of global-scale deforestation: radiative versus nonradiative processes, J. Climate, 23, 97–112, 2010. 14642, 14643, 14660

DeFries, R. and Townsend, J.: NDVI-derived land-cover classifications at a global-scale, Int. J. Remote Sens., 15, 3567–3586, 1994. 14645

Diochon, A., Kellman, L., and Beltrami, H.: Looking deeper: an investigation of soil carbon losses following harvesting from a managed northeastern red spruce (*Picea rubens Sarg.*) forest chronosequence, Forest Ecol. Manag., 257, 413–420, 2009. 14658, 14662, 14665

Durieux, L., Machado, L., and Laurent, H.: The impact of deforestation on cloud cover over the Amazon arc of deforestation, Remote Sens. Environ., 86, 132–140, 2003. 14644, 14663

Foley, J. A., Ramankutty, N., Brauman, K. A., Cassidy, E. S., Gerber, J. S., Johnston, M., Mueller, N. D., O'Connell, C., Ray, D. K., West, P. C., Balzer, C., Bennett, E. M., Carpenter, S. R., Hill, J., Monfreda, C., Polasky, S., Rockström, J., Sheehan, J., Siebert, S., Tilman, D., and Zaks, D. P. M.: Solutions for a cultivated planet, Nature, 478, 337–342, 2011. 14641

Food and A. O. of the United Nations: Global Forest Resources Assessment 2010: Global Tables, available at: http://www.fao.org/forestry/fra/fra2010/en/, 2010. 14641

Forster, P., Ramaswamy, V., Artaxo, P., Berntsen, T., Betts, R., Fahey, D., Haywood, J., Lean, J., Lowe, D., Myhre, G., Nganga, J., Prinn, R., Raga, G., Schulz, M., and Dorland, R. V.: Climate Change 2007: The Physical Science Basis. Contribution of Working Group I to the Fourth Assessment Report of the Intergovernmental Panel on Climate Change, Cambridge University Press, Cambridge, UK, and New York, NY, USA, 2007. 14652

Friedlingstein, P. and Prentice, I. C.: Carbon-climate feedbacks: a review of model and observation based estimates, Curr. Opin. Environ. Sustain., 2, 251–257, 2010. 14652





BGD

9, 14639–14687, 2012



Friedlingstein, P., Joel, G., Field, C., and Fung, I.: Toward an allocation scheme for global terrestrial carbon models, Glob. Change Biol., 5, 755–770, 1999. 14641

Friedlingstein, P., Cox, P., Betts, R., Bopp, L., Von Bloh, W., Brovkin, V., Cadule, P., Doney, S., Eby, M., Fung, I., Bala, G., John, J., Jones, C., Joos, F., Kato, T., Kawamiya, M., Knorr, W., Lindsay, K., Matthews, H. D., Raddatz, T., Rayner, P., Reick, C., Roeckner, E., Schnitzler, K. G., Schnur, R., Strassmann, K., Weaver, A. J., Yoshikawa, C., and Zeng, N.: Climate-carbon cycle feedback analysis: results from the (CMIP)-M-4 model intercomparison, J. Climate, 19, 3337–3353, 2006. 14660

Gibbs, H. K., Ruesch, A. S., Achard, F., Clayton, M. K., Holmgren, P., Ramankutty, N., and Foley, J. A.: Tropical forests were the primary sources of new agricultural land in the 1980s and 1990s, P. Natl. Acad. Sci. USA, 107, 16732–16737, 2010. 14641

Gotelli, N. J.: A Primer of Ecology, Sinauer Associates, Sunderland, MA, USA, 2001. 14645

Govindasamy, B., Duffy, P., and Caldeira, K.: Land use changes and Northern Hemisphere cooling, Geophys. Res. Lett., 28, 291–294, 2001. 14642

Houghton, R.: Revised estimates of the annual net flux of carbon to the atmosphere from changes in land use and land management 1850–2000, Tellus B, 55, 378–390, 2003. 14645

Kleidon, A., Fraedrich, K., and Heimann, M.: A green planet versus a desert world: estimating the maximum effect of vegetation on the land surface climate, Clim. Change, 44, 471–493, 2000. 14641, 14642

Lee, X., Goulden, M. L., Hollinger, D. Y., Barr, A., Black, T. A., Bohrer, G., Bracho, R., Drake, B., Goldstein, A., Gu, L., Katul, G., Kolb, T., Law, B. E., Margolis, H., Meyers, T., Monson, R., Munger, W., Oren, R., Paw U, K. T., Richardson, A. D., Schmid, H. P., Staebler, R., Wofsy, S., and Zhao, L.: Observed increase in local cooling effect of deforestation at higher latitudes, Nature, 479, 384–387, 2011. 14659

Magrin, G., Garcia, C., Choque, D., J. C., Giménez, Moreno, A., Nagy, G., Nobre, C., and Villamizar, A.: Climate Change 2007: Impacts, Adaptation and Vulnerability. Contribution of Working Group II to the Fourth Assessment Report of the Intergovernmental Panel on Climate Change, Cambridge University Press, Cambridge, UK, 2007. 14641

Marland, G., Boden, T., and Andres, R.: Global, regional, and national annual $CO_2$ emissions from fossil-fuel burning, cement production, and gas flaring: 1751–1999., Tech. rep., CDIAC NDP-030, Carbon Dioxide Information Analysis Center, Oak Ridge National Laboratory, available at: http://cdiac.ornl.gov/ndps/ndp030.html, 2002. 14645





BGD
9, 14639–14687, 2012



Matthews, H. D., Weaver, A. J., Meissner, K. J., Gillett, N. P., and Eby, M.: Natural and anthropogenic climate change: incorporating historical land cover change, vegetation dynamics and the global carbon cycle., Clim. Dynam., 22, 461–479, 2004. 14642, 14661

McCarthy, J. J., Canziani, O. F., Leary, N., Dokken, D., and White, K.: Climate Change 2001: Impacts, Adaptation and Vulnerability, Contribution of Working Group II to the Third Assessment Report of the Intergovernmental Panel on Climate Change, Cambridge University Press, Cambridge, UK, 2001. 14641

Meissner, K., Weaver, A., Matthews, H., and Cox, P.: The role of land surface dynamics in glacial inception: a study with the UVic Earth System Model, Clim. Dynam., 21, 515–537, doi:10.1007/s00382-003-0352-2, 2003. 14661

Monfreda, C., Ramankutty, N., and Foley, J. A.: Farming the planet: 2. Geographic distribution of crop areas, yields, physiological types, and net primary production in the year 2000, Global Biogeochem. Cy., 22, 2008. 14641

Montenegro, A., Eby, M., Mu, Q., Mulligan, M., Weaver, A. J., Wiebe, E. C., and Zhao, M.: The net carbon drawdown of small scale afforestation from satellite observations, Global Planet. Change, 69, 195–204, 2009. 14643, 14644, 14663

Nakićenović, N. and Swart, R.: Special Report on Emissions Scenarios, Cambridge University Press, Cambridge, UK, 2000. 14645

Nave, L. E., Vance, E. D., Swanston, C. W., and Curtis, P. S.: Harvest impacts on soil carbon storage in temperate forests, Forest Ecol. Manag., 259, 857–866, 2010. 14662, 14665

Oschlies, A. and Garcon, V.: An eddy-permitting coupled physical-biological model of the North Atlantic – 1. Sensitivity to advection numerics and mixed layer physics, Global Biogeochem. Cy., 13, 135–160, 1999. 14644

Poeplau, C., Don, A., Vesterdal, L., Leifeld, J., Van Wesemael, B., Schumacher, J., and Gensior, A.: Temporal dynamics of soil organic carbon after land-use change in the temperate zone – carbon response functions as a model approach, Glob. Change Biol., 17, 2415–2427, 2011. 14658, 14662, 14665

Pongratz, J., Reick, C. H., Raddatz, T., Caldeira, K., and Claussen, M.: Past land use decisions have increased mitigation potential of reforestation, Geophys. Res. Lett., 38, L15701, doi:10.1029/2011GL047848, 2011. 14643

Ramankutty, N. and Foley, J.: Estimating historical changes in global land cover: croplands from 1700 to 1992, Global Biogeochem. Cy., 13, 997–1027, 1999. 14641, 14645





BGD
9, 14639–14687, 2012



Ramankutty, N., Evan, A. T., Monfreda, C., and Foley, J. A.: Farming the planet: 1. Geographic distribution of global agricultural lands in the year 2000, Global Biogeochem. Cy., 22, GB1003, doi:10.1029/2007GB002952, 2008. 14640, 14641

Roy, J., Saugier, B., and Mooney, H.: Terrestrial Global Productivity, Physiological Ecology, Academic Press, San Diego, CA, USA, 2001. 14653

Schmidt, M. W. I., Torn, M. S., Abiven, S., Dittmar, T., Guggenberger, G., Janssens, I. A., Kleber, M., Koegel-Knabner, I., Lehmann, J., Manning, D. A. C., Nannipieri, P., Rasse, D. P., Weiner, S., and Trumbore, S. E.: Persistence of soil organic matter as an ecosystem property, Nature, 478, 49–56, 2011. 14660, 14665

Schmittner, A., Oschlies, A., Giraud, X., Eby, M., and Simmons, H.: A global model of the marine ecosystem for long-term simulations: sensitivity to ocean mixing, buoyancy forcing, particle sinking, and dissolved organic matter cycling, Global Biogeochem. Cy., 19, GB3004, doi:10.1029/2004GB002283, 2005. 14644

Shukla, J., Nobre, C., and Sellers, P.: Amazon deforestation and climate change, Science, 247, 1322–1325, 1990. 14663

Sitch, S., Huntingford, C., Gedney, N., Levy, P. E., Lomas, M., Piao, S. L., Betts, R., Ciais, P., Cox, P., Friedlingstein, P., Jones, C. D., Prentice, I. C., and Woodward, F. I.: Evaluation of the terrestrial carbon cycle, future plant geography and climate-carbon cycle feedbacks using five Dynamic Global Vegetation Models (DGVMs), Glob. Change Biol., 14, 2015–2039, 2008. 14655

Walker, I. and Sydneysmith, R.: British Columbia, in: From Impacts to Adaptation: Canada in a Changing Climate, Government of Canada, Ottawa, ON, 329–386, 2007. 14641

Weaver, A., Eby, M., Wiebe, E., Bitz, C., Duffy, P., Ewen, T., Fanning, A., Holland, M., MacFadyen, A., Matthews, H., Meissner, K., Saenko, O., Schmittner, A., Wang, H., and Yoshimori, M.: The UVic Earth System Climate Model: model description, climatology, and applications to past, present and future climates, Atmos. Ocean, 39, 361–428, 2001. 14644

Zhang, H., Henderson-Sellers, A., and McGuffie, K.: The compounding effects of tropical deforestation and greenhouse warming on climate, Clim. Change, 49, 309–338, 2001. 14643





BGD
9, 14639–14687, 2012



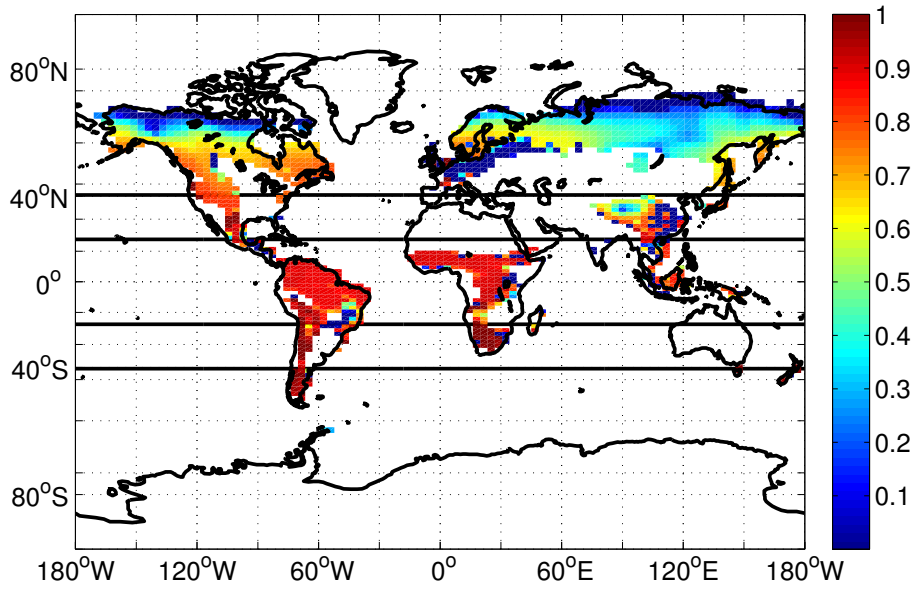


**Fig. 1.** 2010 Forest Coverage. Coverage is represented as fractional amount of broadleaf and needleleaf trees in each grid cell. Latitude bands designated by black lines. 40° N and above for the high latitudes, 20–40° N and 20–40° S for the mid latitudes and 20° S to 20° N for the low latitudes.





BGD
9, 14639–14687, 2012



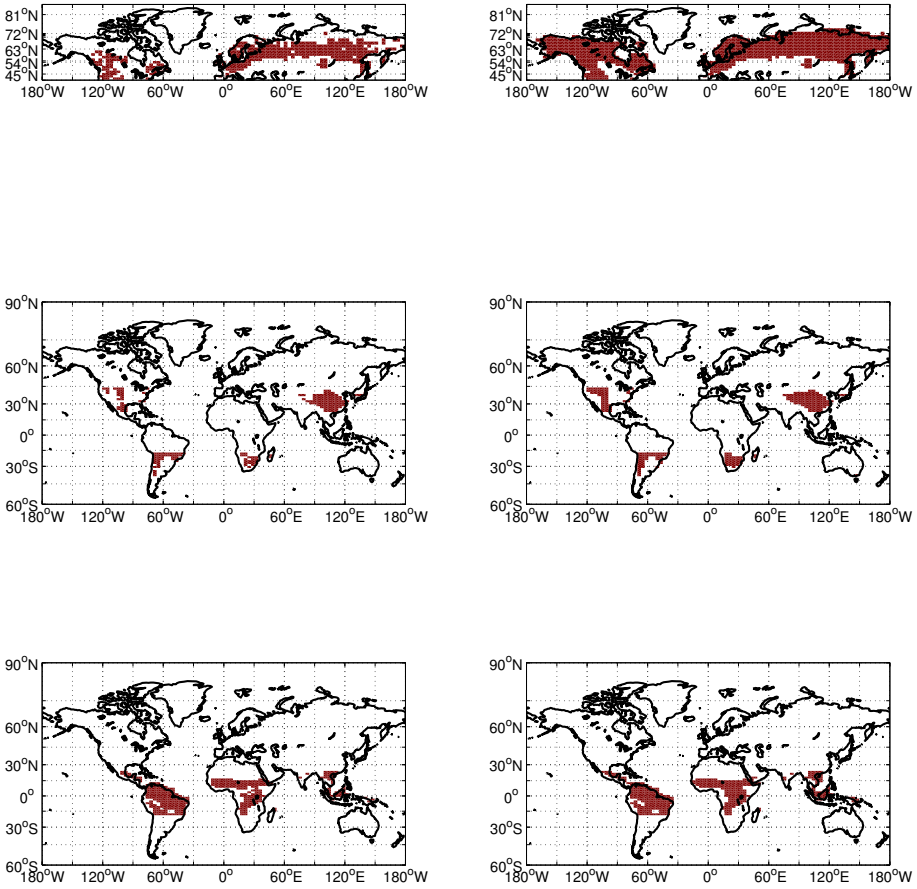


**Fig. 2.** Grid cells eligible for deforestation in the high (top row), mid (middle row) and low latitudes (bottom row) in the non 100 % simulations (left column) and 100 % simulations (right column).





BGD
9, 14639–14687, 2012



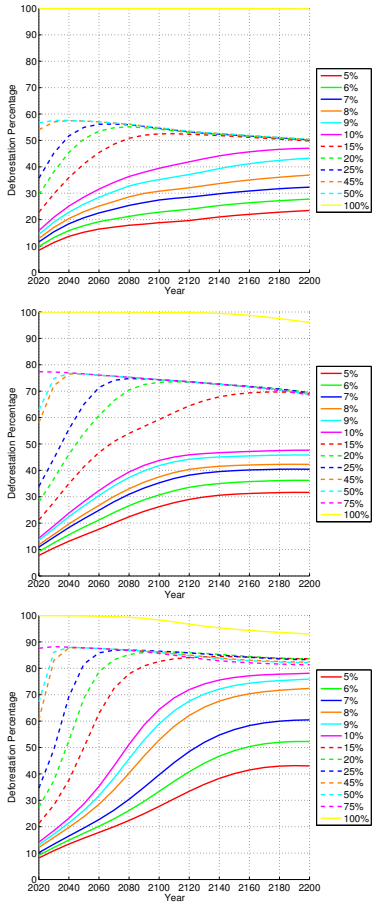


**Fig. 3.** Annually averaged latitudinal forest coverage for high (top), mid (middle), and low latitude (bottom) deforestation simulations. Deforestation percentage is relative to the control run at the same time step.





BGD
9, 14639–14687, 2012



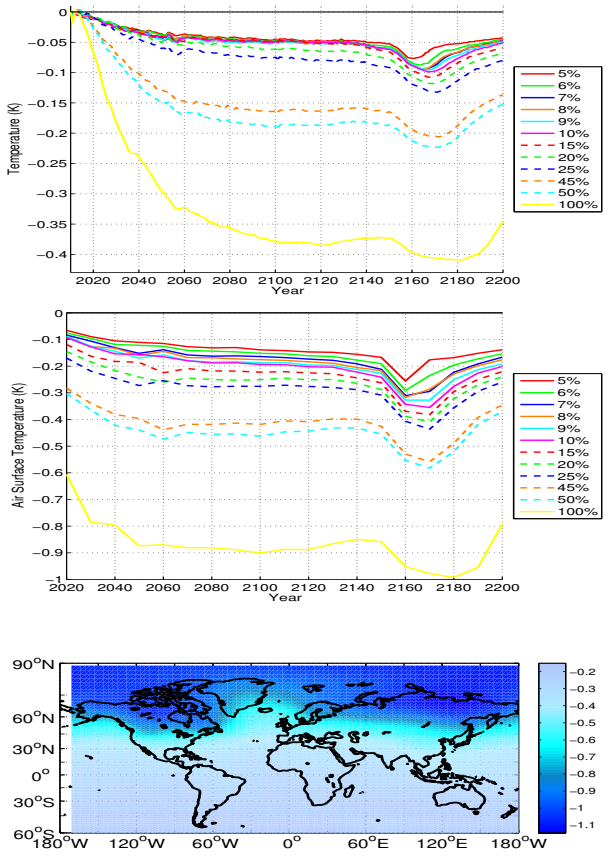


**Fig. 4.** Annually averaged global air surface temperature anomalies for high latitude deforestation (top). Annually averaged air surface temperature anomalies over deforested areas for high latitude deforestation (middle). Air surface temperature anomalies at 2100 for the 100 % high latitude deforestation simulation (bottom). All anomalies are shown in K.





BGD
9, 14639–14687, 2012



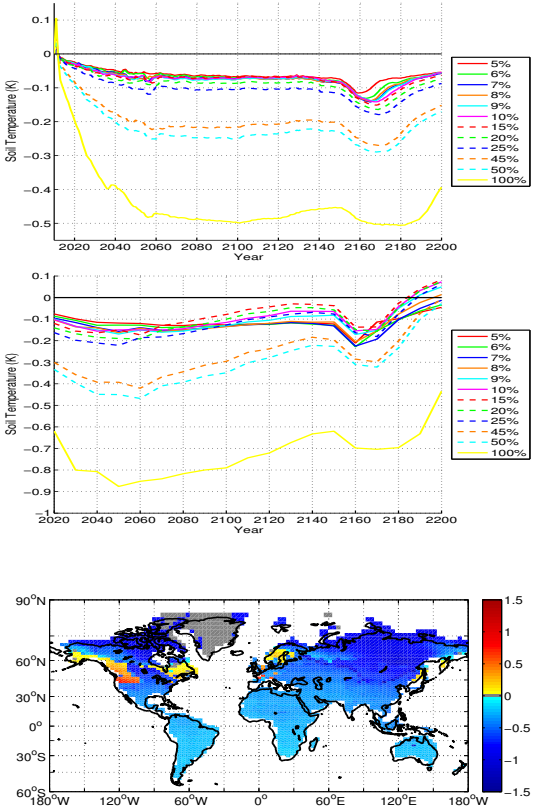


**Fig. 5.** Annually averaged global soil temperature anomalies for high latitude deforestation (top). Annually averaged soil temperature anomalies over deforested areas for high latitude deforestation (middle). Soil temperature anomalies at 2100 for the 100 % high latitude deforestation simulation (bottom). All anomalies are shown in K.





BGD
9, 14639–14687, 2012



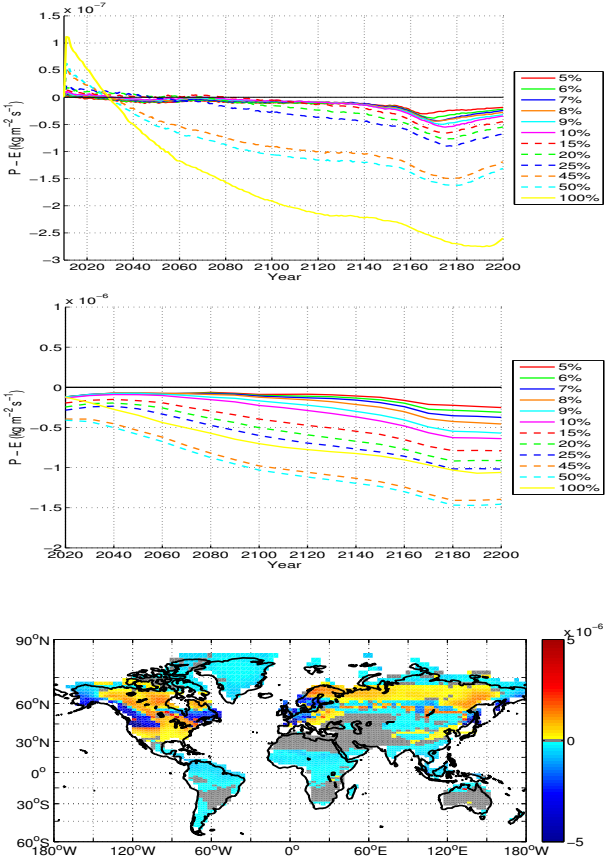


**Fig. 6.** Annually averaged global precipitation minus evapotranspiration anomalies over land for high latitude deforestation (top). Annually averaged precipitation minus evapotranspiration anomalies over deforested areas for high latitude deforestation (middle). Precipitation minus evapotranspiration anomalies at 2100 for the 100 % high latitude deforestation simulation (bottom). All anomalies are shown in kg $m^{-2}$ $s^{-1}$.





BGD
9, 14639–14687, 2012



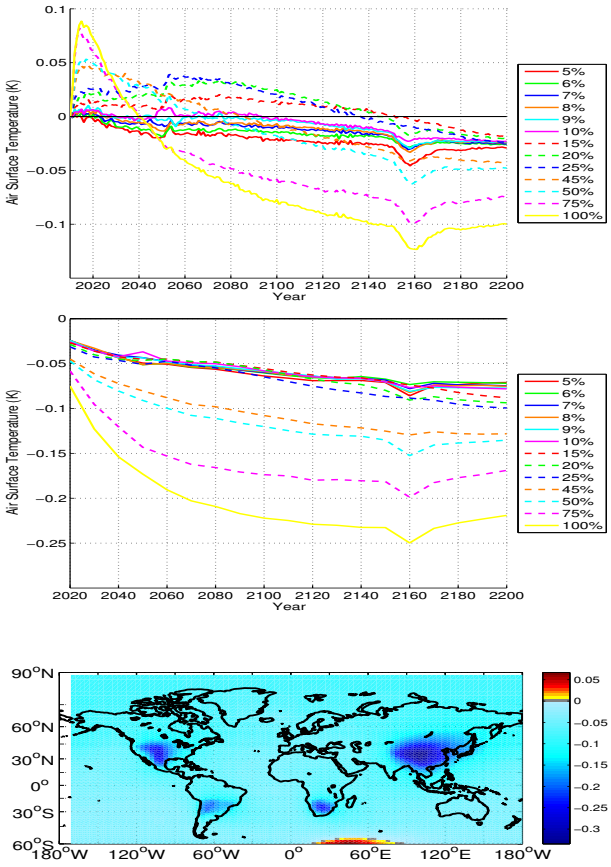


**Fig. 7.** Annually averaged global air surface temperature anomalies for mid latitude deforestation (top). Annually averaged air surface temperature anomalies over deforested areas for mid latitude deforestation (middle). Air surface temperature anomalies at 2100 for the 100 % mid latitude deforestation simulation (bottom). All anomalies are shown in K.





BGD
9, 14639–14687, 2012



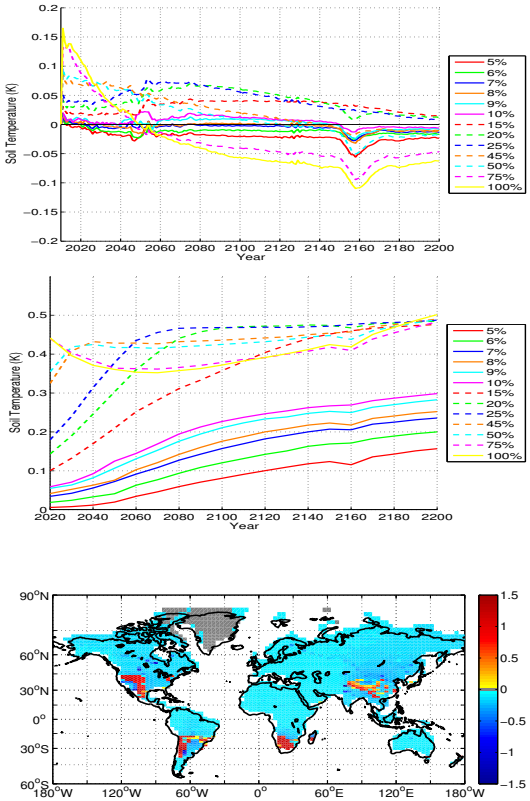


**Fig. 8.** Annually averaged global soil temperature anomalies for mid latitude deforestation (top). Annually averaged soil temperature anomalies over deforested areas for mid latitude deforestation (middle). Soil temperature anomalies at 2100 for the 100 % mid latitude deforestation simulation (bottom). All anomalies are shown in K.





BGD
9, 14639–14687, 2012



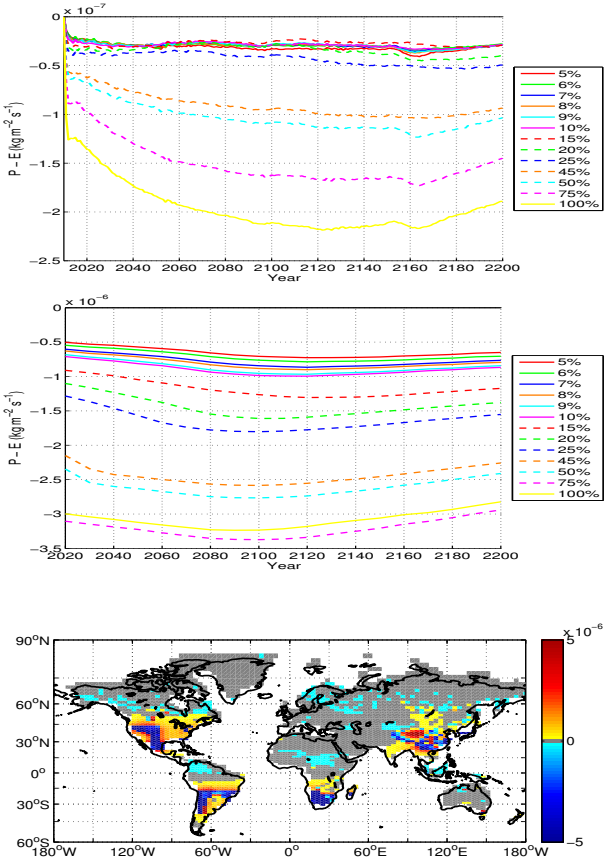


**Fig. 9.** Annually averaged global precipitation minus evapotranspiration anomalies over land for mid latitude deforestation (top). Annually averaged precipitation minus evapotranspiration anomalies over deforested areas for mid latitude deforestation (middle). Precipitation minus evapotranspiration anomalies at 2100 for the 100 % mid latitude deforestation simulation (bottom). All anomalies are shown in kg m$^{-2}$ s$^{-1}$.





BGD
9, 14639–14687, 2012



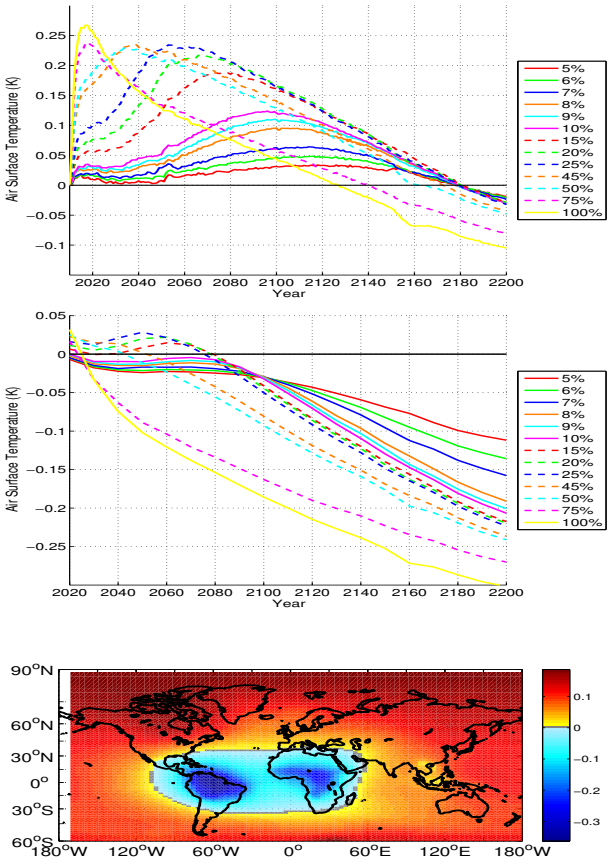


**Fig. 10.** Annually averaged global air surface temperature anomalies for low latitude deforestation (top). Annually averaged air surface temperature anomalies over deforested areas for low latitude deforestation (middle). Air surface temperature anomalies at 2100 for the 100 % low latitude deforestation simulation (bottom). All anomalies are shown in K.





BGD
9, 14639–14687, 2012



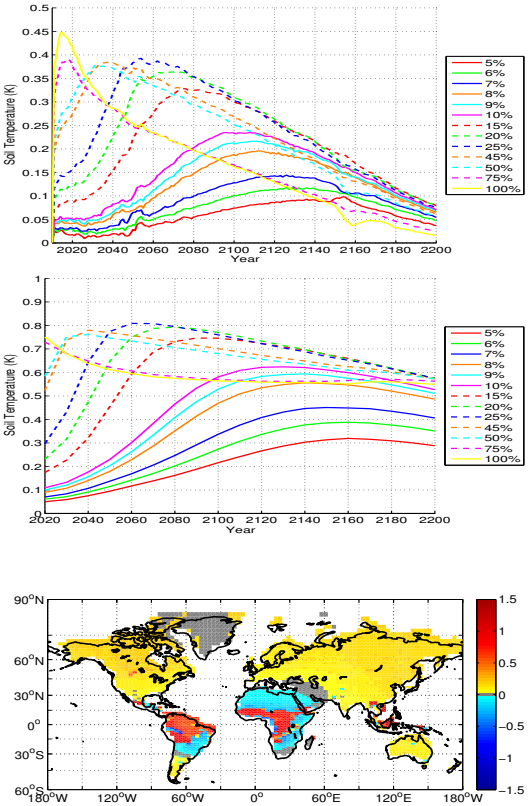


**Fig. 11.** Annually averaged global soil temperature anomalies for low latitude deforestation (top). Annually averaged soil temperature anomalies over deforested areas for low latitude deforestation (middle). Soil temperature anomalies at 2100 for the 100 % low latitude deforestation simulation (bottom). All anomalies are shown in K.





BGD
9, 14639–14687, 2012



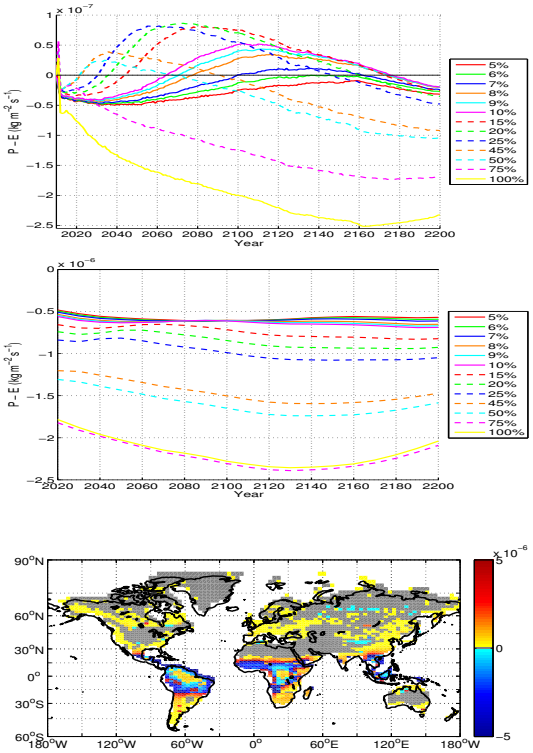


**Fig. 12.** Annually averaged global precipitation minus evapotranspiration anomalies over land for low latitude deforestation (top). Annually averaged precipitation minus evapotranspiration anomalies over deforested areas for low latitude deforestation (middle). Precipitation minus evapotranspiration anomalies at 2100 for the 100 % low latitude deforestation simulation (bottom). All anomalies are shown in kg m$^{-2}$ s$^{-1}$.





BGD
9, 14639–14687, 2012



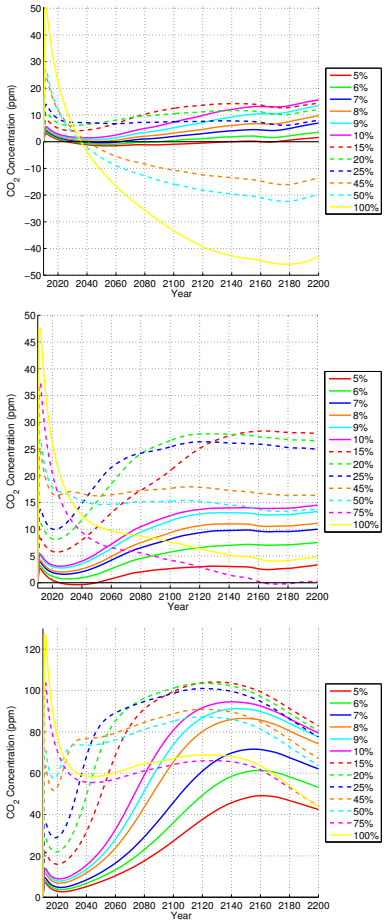


**Fig. 13.** Annually averaged global $CO_2$ concentration anomalies for high (top), mid (middle), and low latitude (bottom) deforestation. All anomalies shown in ppm.





BGD
9, 14639–14687, 2012



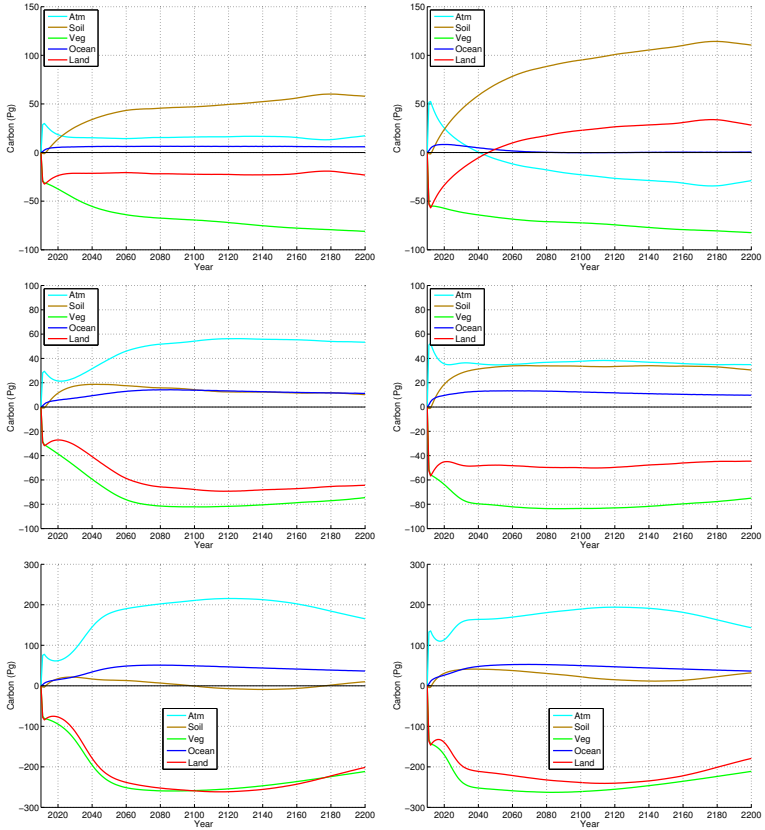


**Fig. 14.** Temporal evolution of annually averaged carbon stock anomalies from different model components for high (top row), mid (middle row), and low latitude (bottom row) simulations for the 25 % (left column) and 45 % deforestation (right column) scenarios. All anomalies shown in Pg C.





BGD
9, 14639–14687, 2012



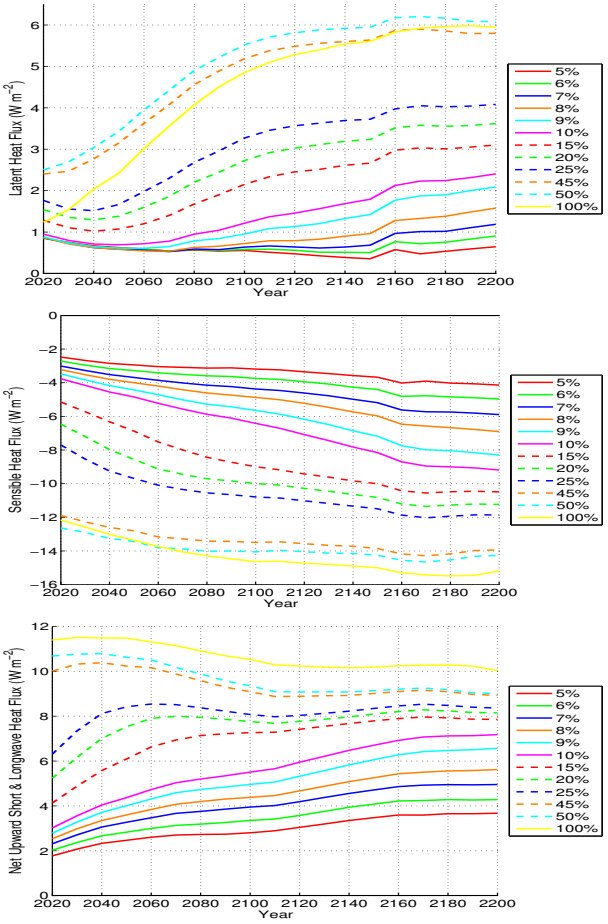


**Fig. 15.** Annually averaged outgoing surface energy flux anomalies over deforested areas for high latitude deforestation. Energy fluxes shown as latent heat (top), sensible heat (middle), and net surface radiation (bottom). All anomalies shown in W m$^{-2}$.





BGD
9, 14639–14687, 2012



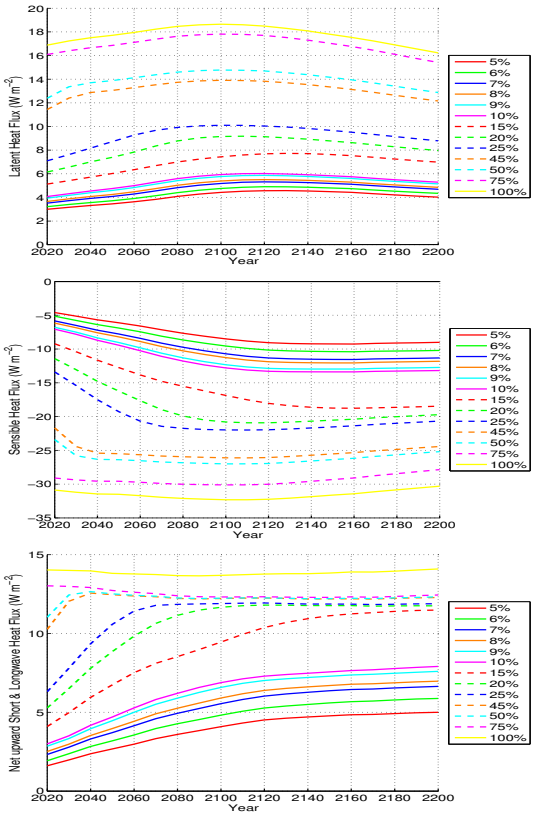


**Fig. 16.** Annually averaged outgoing surface energy flux anomalies over deforested areas for mid latitude deforestation. Energy fluxes shown as latent heat (top), sensible heat (middle), and net surface radiation (bottom). All anomalies shown in W m$^{-2}$.





BGD
9, 14639–14687, 2012



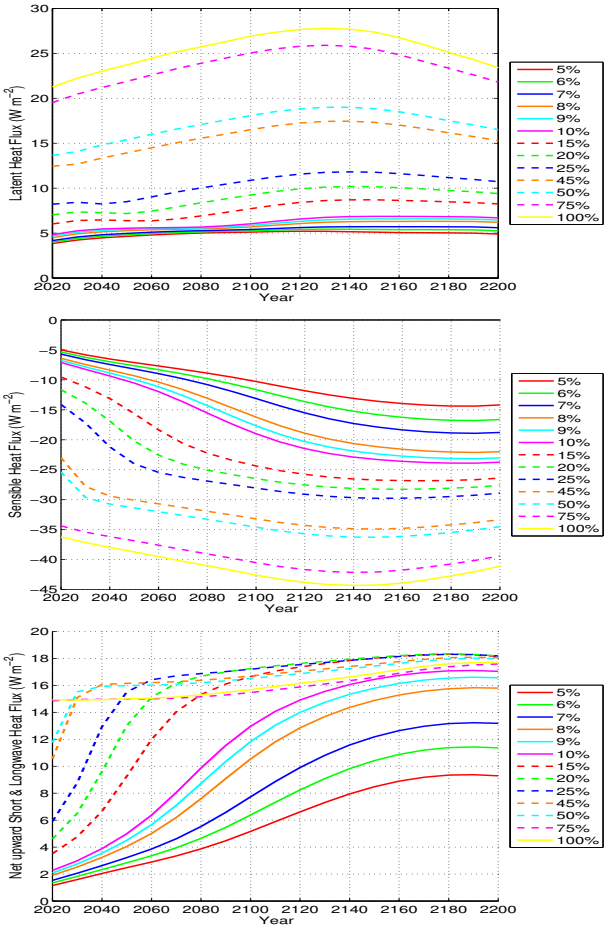


**Fig. 17.** Annually averaged outgoing surface energy flux anomalies over deforested areas for low latitude deforestation. Energy fluxes shown as latent heat (top), sensible heat (middle), and net surface radiation (bottom). All anomalies shown in W m$^{-2}$.





BGD
9, 14639–14687, 2012